Journal of Materials Science: Materials in Electronics (2018) 29:3957–3966
https://doi.org/10.1007/s10854-017-8336-x

Comparison of Vickers microhardness of undoped and Ru doped BSCCO glass ceramic materials

O. Ozturk[1,2] · E. Asikuzun[2,3,4] · A. T. Tasci[1] · T. Gokcen[1,5] · H. Ada[6] · H. Koralay[5] · S. Cavdar[5]

Received: 21 September 2017 / Accepted: 25 November 2017 / Published online: 14 December 2017

Abstract
In this study, effect of substitution ratio on the mechanical and structural properties of $Bi_{1-x}Ru_xPb_{0.2}Sr_2CaCu_2O_{10+\delta}$ system, that is prepared in the ratios of x = 0.0, 0.025, 0.050, 0.075, is investigated. Samples are prepared with glass ceramic method and sintered at 845 °C. XRD and SEM measurements are performed for structural analyses, and Vickers micro-hardness measurements are carried out at different applied load ($0.245 \leq F \leq 2.940$ N) in order to investigate the mechanical performance of the Ru doped $Bi_{1-x}Ru_xPb_{0.2}Sr_2CaCu_2O_{10+\delta}$ system. Experimental results of Vickers micro-hardness analyses are performed using the Meyer's law, the proportional samples resistance model, the elastic/plastic deformation model, the Hays–Kendall approach and the indentation induced cracking (IIC) model. All analyses results are exhibited reverse indentation size effect behavior. The measured hardness values increase with increasing the applied load. Finally, IIC model is determined as the most successful model describing the mechanical properties of our samples.

1 Introduction

Glass ceramics are polycrystalline materials, produced from crystallization of specially compound glasses which are suitable for crystallization. Crystallization is provided with an appropriate and careful heat treatment program allowing the nucleation and growth of crystalline phase in the glass. As the grain size of the crystallized phase may be several μm, production of submicron size is also possible. The main effect, in improving the mechanical properties of glass ceramics such as, fracture toughness, impact resistance, abrasion, is the small grain size of collapsed crystals in the main glass [1–4].

Glass–ceramic materials generally are more resistant and have lower density than some metals against chemical effects and corrosion at high temperatures [4]. Nevertheless conventional ceramic materials have low toughness and ductility (fragile and brittle). So the usage areas and aims of these materials are limited. To improve these limitations, the mechanical and micro-structure properties of ceramic materials should be developed. The most important group among advanced technology ceramics is the glass ceramic material that is used instead of metals in industrial applications by improving mechanical properties [5–15]. Therefore, it is believed that the investigation of mechanical characterizations as well as the microstructure analyses of the glass ceramic material produced will provide important contribution to the literature [16].

To perform the microhardness measurements, there are different methods such as Brinell, Knoop, Rockwell and Vickers microhardness test methods. In this study, Vickers microhardness test method, the most common method, is used to determine of mechanical characterization [17, 18].

✉ E. Asikuzun
easikuzun@kastamonu.edu.tr

1 Department of Physics, Faculty of Arts and Sciences, Kastamonu University, Kastamonu, Turkey

2 Research and Application Center, Kastamonu University, Kastamonu, Turkey

3 Department of Materials Science and Nanotechnology Engineering, Faculty of Engineering and Architecture, Kastamonu University, 37100 Kastamonu, Turkey

4 Department of Physics, Faculty of Arts and Sciences, Abant Izzet Baysal University, Bolu, Turkey

5 Department of Physics, Faculty of Sciences, Gazi University, Ankara, Turkey

6 Department of Machine Engineering, Faculty of Engineering and Architecture, Kastamonu University, Kastamonu, Turkey

2 Experimental details

In the $Bi_{1.8-x}Ru_xPb_{0.2}Sr_2CaCu_2O_{10+\delta}$ (x = 0.0, 0.025, 0.050, 0.075) glass–ceramic structure, high purity Bi_2O_3, PbO, $SrCO_3$, CaO, RuO_2 and CuO powders (Alfa Aesar) are weighed in appropriate stoichiometric proportions. Three grams of powder are prepared for each rate of contribution. For example, 0.075 g Ru and 2.925 g Bi_2O_3 powder for 0.025% Ru doped; 0.150 g Ru and 2.850 g of Bi_2O_3 powder were used for 0.050% Ru doped; 0.225 g Ru and 2.775 g of Bi_2O_3 powder were used for 0.075% Ru doped. All bulk samples are named as Ru0 (undoped sample), Ru025 (0.025% Ru doped), Ru050 (0.050% Ru doped) and Ru075 (0.075% Ru) in other sections.

Chemical powders are mixed by grinding in the agate mortar for about 4 h. The obtained mixture is placed into the furnace in alumina crucibles, and heated up to 1150 °C from the room temperature by heating rate of 10 °C/min. The mixture is annealed for 1.5 h at this temperature. The melting material is poured between two cooled copper plates. As a result of this process, about 1–2 mm thick black glass is obtained. The obtained samples are sintered at 845 °C for 120 h under oxygen flow into the tube furnace from room temperature with rate of 10 °C/min. As a result of this process ceramic samples are obtained.

The determination of the crystal structure and lattice parameters belonging to the samples studied in this work is carried out by a Bruker D8 Advance model diffractometer with CuK_α radiation (λ = 1.5418 Å) in the range 2θ = 5°–60° at a scan speed of 1.2°/min and a step increment of 0.08° at room temperature. SEM analyses are performed in order to investigate the surface morphology of samples by using a JEOL JSM-7000F model scanning electron microscope. Vickers microhardness measurements are made on the sample surfaces at the room temperature to investigate the effect of Ru addition on the mechanical properties using a digital microharness tester (SHIMADZU). The load is applied for 10 s and changed in the range 0.245–2.940 N.

3 Results and discussion

3.1 XRD measurements

The XRD patterns of the Ru0, Ru025, Ru050 and Ru075 samples prepared using the glass ceramic method at 845 °C for 120 h under oxygen flow are given in Fig. 1. When the Ru0 sample is analyzed by XRD, it is determined that the main phase is $Bi_{1.6}Pb_{0.4}Sr_2CaCu_2O_x$ (045-0676-ICDD). The XRD peaks show that there are many

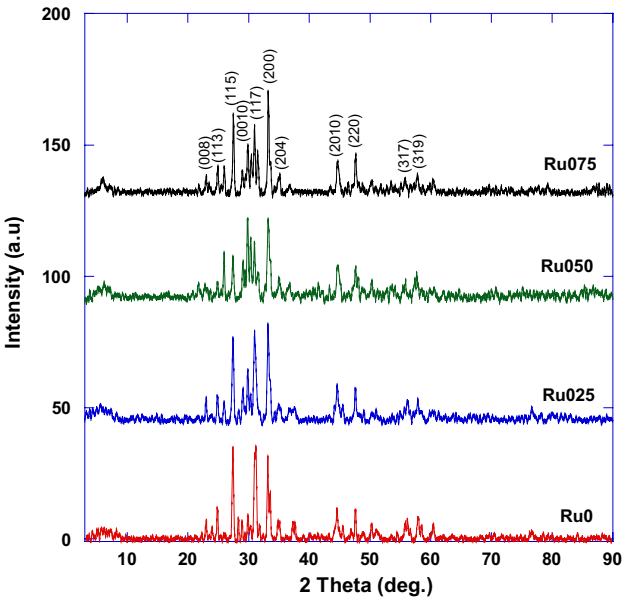

Fig. 1 XRD patterns of all samples

Table 1 *a*, *b* and *c* parameters and volume fracture values of all samples

Samples	$a=b$ (Å)	c (Å)	$V=a*b*c$
Ru0	5.401	30.874	900.619
Ru025	5.398	30.796	897.346
Ru050	5.375	30.902	892.778
Ru075	5.384	30.784	892.350

phases such as Bi-2212 (045-1058-ICDD), Bi-2201 (047-0737-ICDD) phases seperated from main structure and Sr_3PbO (083-1866-ICDD), $SrBi_4O_7$ (046-0752-ICDD) and $Ca_6Sr_8Cu_{24}O_{41}$ (048-1502-ICDD) impurity phases.

As the amount of doping increases, the sample shifts from the low temperature phase (% V2212) to the very low temperature phase (% V2201). But the dominant phase is the low temperature phase (% V2212). Furthermore, no secondary phase containing Ru or any other cation is observed even up to x = 0.075, showing that the Ru atoms are successfully introduced to the microstructure of the Bi-2212 phase.

Furthermore, lattice parameters *a* and *c* of all samples are calculated and given in the Table 1. All samples prepared have tetragonal crystal structure. As seen from the table, *a* and *c* parameters of the samples decrease with increasing the doping. *a* parameter decreases to 5.38 from 5.40 Å and *c* parameter decreases to 30.78 from 30.87 Å. While the lattice volume is 900.619 Å for undoped sample, this value decrease to 892.350 Å for Ru075 sample.

3.2 SEM measurements

Surface morphology of the samples, prepared with glass ceramic method, is performed by JEOL JSM-7000F scanning electron microscopy. From the SEM images (Fig. 2), it is observed that grain sizes decrease with increasing Ru doping. Although samples are annealed at the same temperature, melting is observed in Ru075 samples. This means that increasing of doping is decreased resistance of structure. It is observed that the crystallization of the sample decreases depending on the doping rate. As a result of this, plate and needle like structures occur only in the undoped sample (Ru0). Increasing the doping rate prevents the formation of acicular structure.

3.3 Vickers microhardness measurements

Microhardness measurements are carried using digital microhardness tester to determine the effect of Ru doping on the mechanical properties of $Bi_{1.8-x}Ru_xPb_{0.2}Sr_2CaCu_2O_y$ (x = 0.0, 0.025, 0.050, 0.075) system at room temperature.

In this study, no polishing or mechanical process has been done before indentation. Measurements are taken from the untreated sample surface. Microhardness values are determined with an average of seven readings at different parts of the sample surfaces making sure that the indentations do not overlap.

The applied load (F) is changed between 0.245 and 2.940 N and applied on the surface of samples for 10 s. The load dependent microhardness (H_v), elastic modulus (E), yield strength (Y), fracture toughness (K_{IC}) values are calculated using Eq. (3–6) and given in the Table 1. In addition,

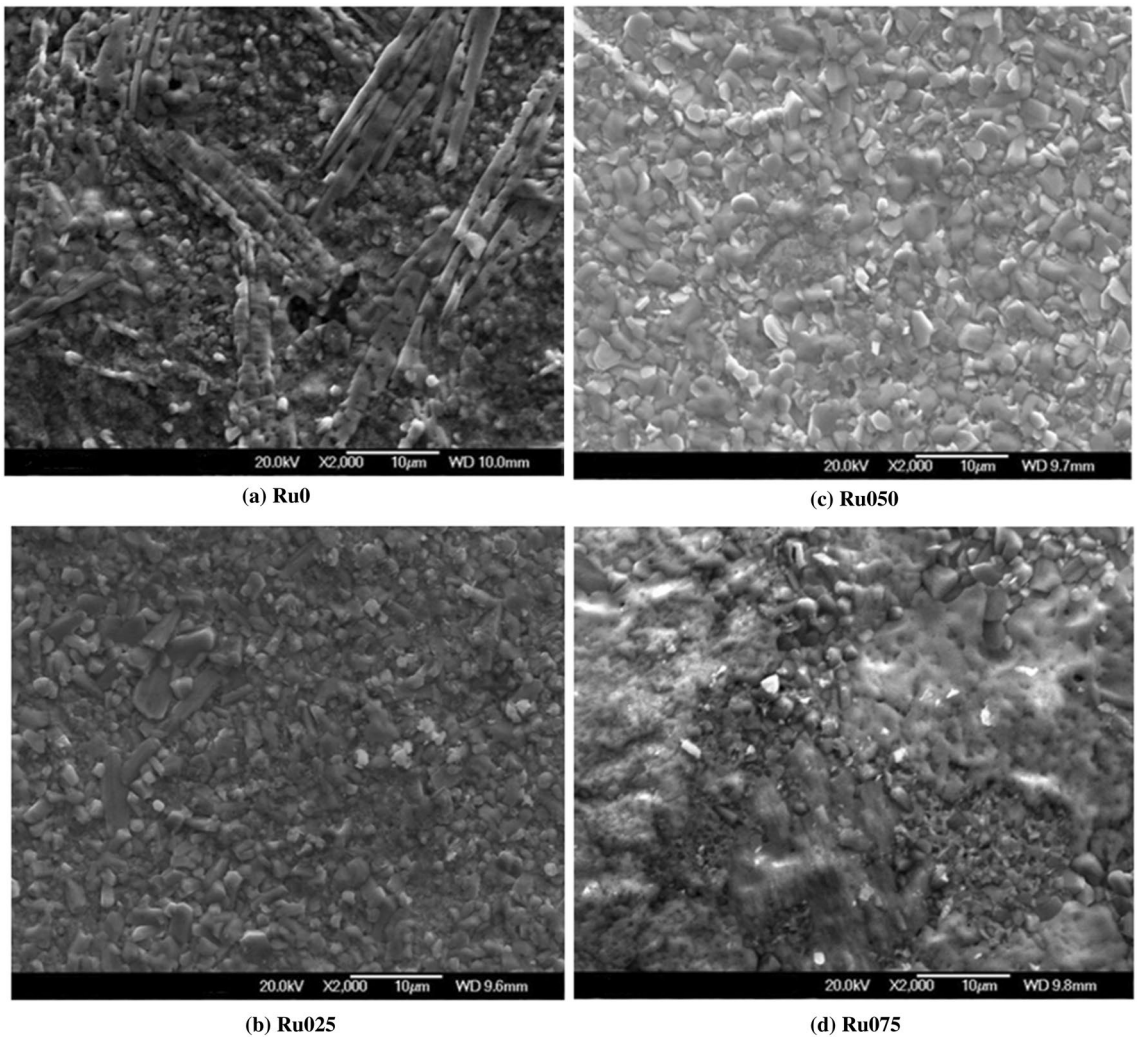

Fig. 2 SEM micrographs of all samples

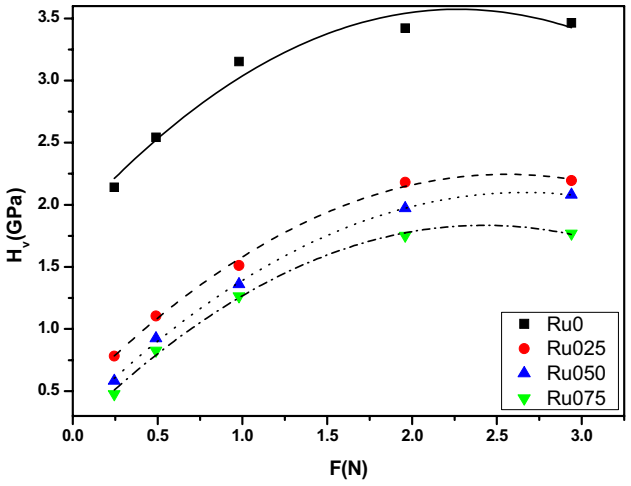

Fig. 3 Variations of microhardness with applied load for the samples

the optical trace photos of the indentations for each sample under 2.940 N load are shown in Fig. 3.

H_v hardness is determined by *F*/*A* ratio. Here, *F* is applied load on the surface of material and *A* is surface area in terms of micrometers square [18–21]. *A* can be calculated by the following formula:

$$A = \frac{d^2}{2\sin(136°/2)} \tag{1}$$

$$A \approx \frac{d^2}{1854.4} \tag{2}$$

In this study, Vickers microhardness test method is used for hardness measurements. The pyramid-shaped indentation tip is used in the measurements. The apex angle of pyramid made from diamond is α = 136° (Table 2).

The Vickers microhardness values (H_v) of different applied loads in the range of 0.245–2.940 N for a peak-load time of 10 s, were calculated by using Eq. 3. The Vickers microhardness values were calculated with an average of 7 readings.

$$H_v = F/A \approx 1854.4\frac{F}{d^2} \tag{3}$$

$$E = 81.9635\,H_v \tag{4}$$

Here, the constant 81.9635 in Eq. 4 is a constant used for the elastic modulus calculations of ceramic materials in the literature [18, 19].

$$Y \approx \frac{H_v}{3} \tag{5}$$

Yield strength (Y) is the indication of maximum stress that can be developed in a material without causing plastic deformation and can be calculated by using Eq. (5) [20, 21].

Table 2 H_v, *E, Y* and K_{IC} load-dependent values of samples

Samples	*F* (N)	H_V (GPa)	*E* (GPa)	*Y* (GPa)	*Kıc* (Pa/m$^{1/2}$)
Ru0	0.245	2.14	175.402	0.713	−242.114
	0.490	2.543	208.433	0.848	−263.931
	0.980	3.152	258.349	1.051	−293.836
	1.960	3.421	280.397	1.140	−306.120
	2.940	3.464	283.922	1.155	−308.042
Ru025	0.245	0.782	64.095	0.261	−223.047
	0.490	1.106	90.652	0.369	−265.254
	0.980	1.512	123.929	0.504	−310.145
	1.960	2.182	178.844	0.727	−372.585
	2.940	2.195	179.910	0.732	−373.697
Ru050	0.245	0.583	47.785	0.194	−222.013
	0.490	0.925	75.816	0.308	−279.660
	0.980	1.360	111.470	0.453	−339.101
	1.960	1.973	161.714	0.658	−408.436
	2.940	2.08	170.484	0.693	−419.368
Ru075	0.245	0.477	39.097	0.159	−189.631
	0.490	0.826	67.702	0.275	−249.539
	0.980	1.263	103.520	0.421	−308.577
	1.960	1.752	143.600	0.584	−363.428
	2.940	1.769	144.993	0.590	−365.184

Yield strength is very important for engineering structural design. For example, when designing a device, it must support the applied load, and the material must not deform plastically. Therefore, a material with sufficient yield strength should be selected.

$$K_{ic} = \sqrt{2E\gamma} \tag{6}$$

γ (gamma) is the surface energy of crack which is obtained from intercept of the lines in *F*/*d*–*d* graph.

It can be seen from Fig. 3 that the microhardness values increase with increasing applied load. This result indicates that all materials exhibit reverse indentation size effect (RISE) behavior. In addition, the microhardness values decrease with increasing Ru doping. Also, *E, Y* and K_{IC} values, that are important as microhardness in mechanical characterization of the materials, increase with increasing the applied load. Microhardness, *E, Y* and K_{IC} values depend on the applied load as in literature studies [16, 17, 22–24].

3.4 Analyses and modelling of microhardness

3.4.1 Meyer's law

Meyer' s law, used to explain behavior of materials (ISE/RISE) with applied load, is a hardness analysing method. It is given by Eq. (5)

$$F = Ad^{n_k} \tag{7}$$

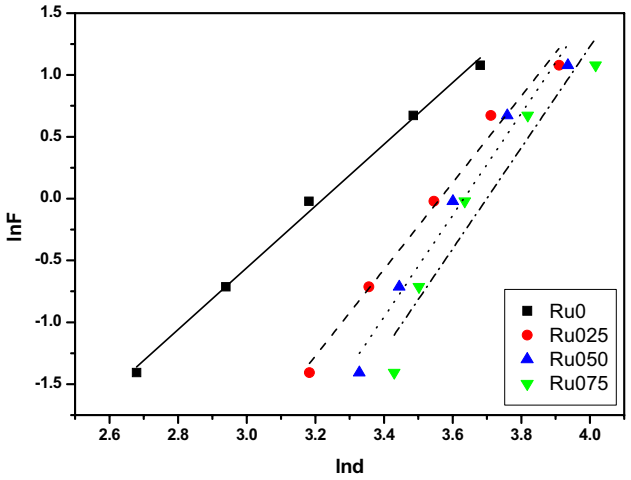

Fig. 4 Variation of applied load *lnF* with diagonal length *lnd* for the samples

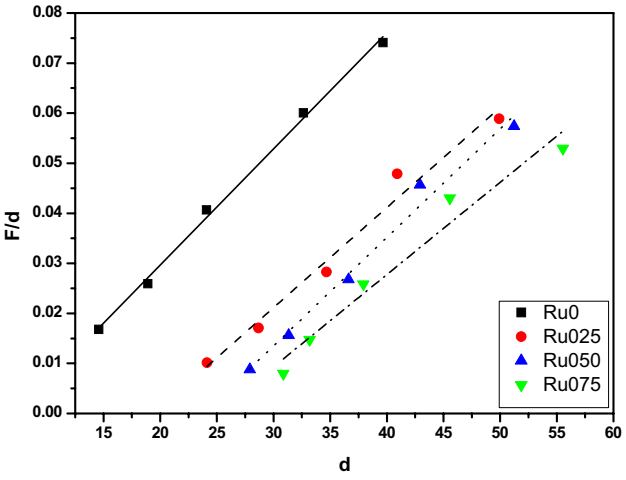

Fig. 5 Plot of *F*/*d* versus *d* for the samples

Table 3 Best-fit results of experimental data according to Meyer's law

Samples	n_K	lnA_{1K} (GPa)	H_V (GPa)
Ru0	2.49	− 8.047	3.421–3.464
Ru025	3.50	− 12.483	2.182–2.195
Ru050	4.11	− 14.941	1.973–2.080
Ru075	4.08	− 15.126	1.752–1.769

Table 4 Best-fit result of experimental data according to PSR model

Samples	$\gamma \times 10^{-3}$ (N/μm)	$\varepsilon \times 10^{-4}$ (N/μm^2)	H_{PSR} (GPa)	H_V (GPa)
Ru0	− 16.71	23.2	4.302	3.421–3.464
Ru025	− 38.81	20.00	3.708	2.182–2.195
Ru050	− 45.47	19.64	3.642	1.973–2.080
Ru075	− 45.99	18.4	3.412	1.752–1.769

here A is a load independent constant and n_k is the Meyer number, which is a measure of ISE or RISE behaviour. If value of n_k is > 2, RISE behaviour is observed, if < 2, ISE behaviour is observed [25–27].

The slope of *InF–Ind* graph (Fig. 4) gives the value of n_k and we can see that, it is > 2 for all samples. It is confirmed that the microhardness increases with applied load and the material exhibits RISE behaviour (Table 3). In addition, as noted in the literature, materials are classified as hard or sorf materials. If value of n_k is between 1 and 1.6, material is hard; if n_k > 1.6, material is soft [28]. According to the obtained results, the produced glass ceramic samples are soft materials. Also, it is shown in the literature that microhardness of glass decreases with lead doping [29]. The BSCCO (Bi–Sr–Ca–Cu–O) material, used in the production of wire and strip, is known as a soft material because of this property. In this study, the value of n_k is > 1.6. So, we can say that, obtained results are consistent with the literature.

3.4.2 PSR model

Proportional samples resistance (PSR) model is developed by Li and Bradt [5] to analyse the indentation size effect (ISE) behavior. This model is expressed by,

$$F = \gamma d + \varepsilon d^2 \tag{8}$$

ε is determined from the slope of *F*/*d*–*d* graph (Fig. 5) [30, 31] and this value is used to calculate the true hardness value. According to the PSR model, load independent microhardness is calculated by Eq. (9).

$$H_{PSR} = 1854.4\,\varepsilon \tag{9}$$

The resulting data are summarized in Table 4. As can be seen from this table, the values of γ are negative, an expected result for materials that exhibit RISE behaviour. This situation confirms that only plastic deformations occur in these samples which shows RISE behavior. There is no elastic deformation. Also, plateau values of samples are far from microhardness values calculated by PSR model [32, 33]. Therefore, PSR model is insufficient to determine the exact hardness values of the materials. The load-independent elastic modulus (E_0), yield strength (Y_0) and fracture toughness (K_{IC}) values are calculated as well as load independent hardness value (H_{PSR}) and given Table 5. In addition, it can be seen that E_o and Y values decrease with increasing the Ru doping (Fig. 6).

Fracture toughness is one of the basic mechanical properties of ceramic samples. It is an important parameter

Table 5 Calculated load-independent H_v, E_0, Y_0 and K_{ic} for the samples

Samples	H_0 (GPa)	E_0 (GPa)	Y_0 (GPa)	K_{IC} (Pa/m$^{1/2}$)	H_V (GPa)
Ru0	4.302	352.607	1.434	−343.177	3.421–3.464
Ru025	3.708	303.920	1.236	−485.636	2.182–2.195
Ru050	3.642	298.510	1.214	−521.018	1.973–2.080
Ru075	3.412	279.659	1.137	−506.682	1.752–1.769

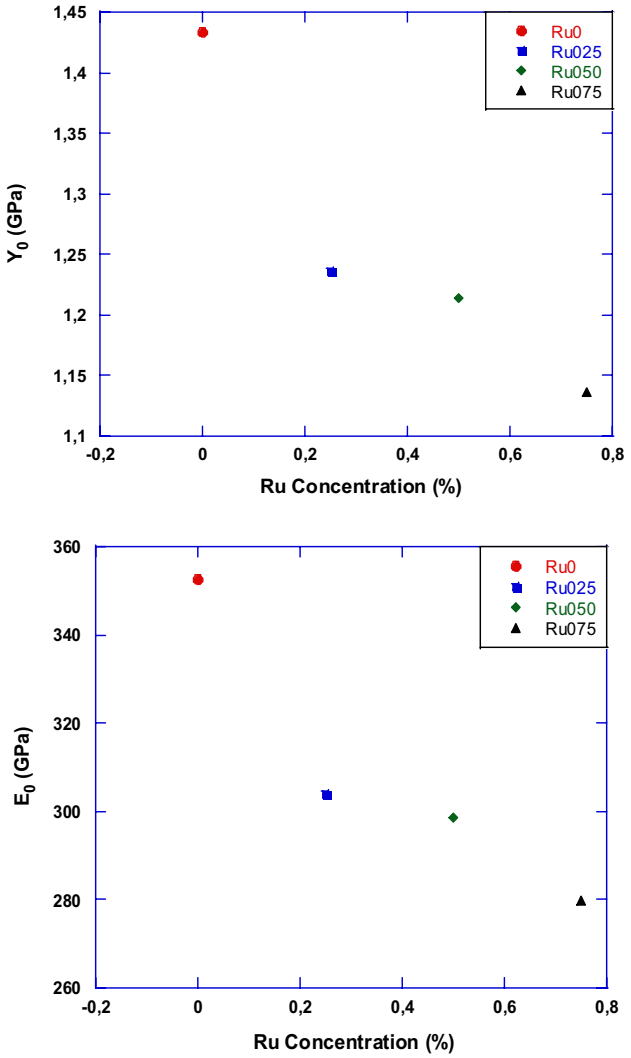

Fig. 6 Variations of load independent **a** Y_0 and **b** E_0 values with Ru concentration for the samples

for the determination of materials that will be used in technological applications. With the increase of the Ru concentration in the BSCCO system, the K_{IC} value tends to increase significantly due to the increment of the surface energy γ. Thus, it can be concluded that, the Ru addition improves the mechanical properties of the BSCCO

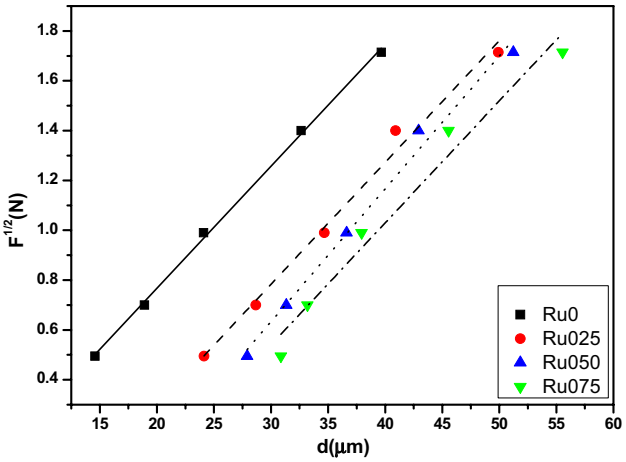

Fig. 7 Plots of square root applied loads versus diagonal length for the samples

Table 6 Best-fit results of experimental data according to EPD model

Samples	$A_2^{1/2}$ (N/μm^2)	d_e (μm)	H_{EPD} (GPa)	H_V (GPa)
Ru0	0.0489	−0.21	4.434	3.421–3.464
Ru025	0.0488	−0.68	4.416	2.182–2.195
Ru050	0.0533	−0.96	5.268	1.973–2.080
Ru075	0.0489	−0.92	4.434	1.752–1.769

superconducting system. The negative K_{IC} and γ values indicates that the material shows RISE behavior. K_{IC} and γ values are positive in materials exhibiting ISE behavior [34, 35].

3.4.3 Elastic/plastic deformation model

According to Bull et al. [36, 37] the correlation between applied load and indentation size is given by,

$$F = A_2(d_e + d_p)^2 \tag{10}$$

here d_e and d_p are indentation size values (Fig. 7), that are formed with elastic and plastic deformation, respectively. In this model, values of the load independent microhardness are calculated by,

$$H_{EPD} = 1854.4\,A_2 \tag{11}$$

As can be seen from Table 6, values of d_e are negative for undoped and Ru doped samples. There is only plastic deformation for all samples. Elastic deformation is not observed. Microhardness values, calculated by elastic/plastic deformation (EPD) model, are far from plateau region where microhardness is not changed with applied load. As a result, it is

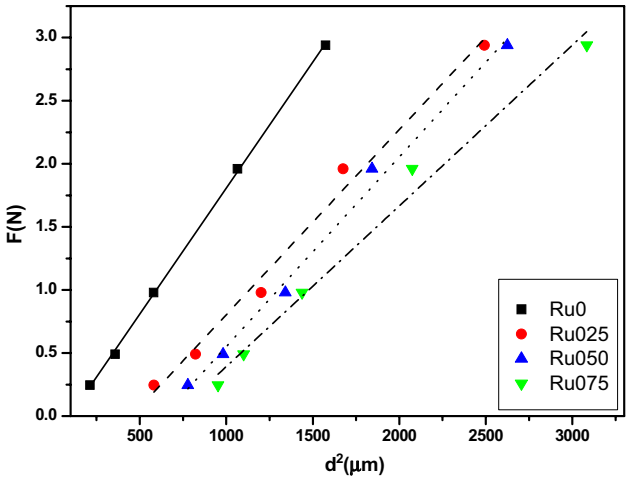

Fig. 8 Applied load versus the square of the impression semi-diagonal length for the samples

Table 7 Best-fit results of experimental data according to HK model

Samples	$A_{1HK} \times 10^{-3}$	W_{HK} (N)	H_{HK} (GPa)	H_V (GPa)
Ru0	2.0	−0.19	3.708	3.421–3.464
Ru025	1.4	−0.66	2.725	2.182–2.195
Ru050	1.5	−0.95	2.781	1.973–2.080
Ru075	1.2	−0.88	2.355	1.752–1.769

clearly observed that the EPD model is not useful to determine the microhardness of the samples.

3.4.3.1 Hays–Kendall approach Hays and Kendall suggested that minimum load value (W) can create permanent deformation in a sample. If the applied load does not exceed this resistance, permanent deformation does not occur and only elastic deformation occurs [38].

$$F - W_{HK} = A_{1HK} d^2 \tag{12}$$

here A_{1HK} is an independent constant from the applied load. W_{HK} and A_{1HK} values are calculated from $F - d^2$ graph (Fig. 8). In this model, load independent microhardness values are calculated by using Eq. 13.

$$H_{HK} = 1854.4 A_{HK} \tag{13}$$

In Table 7, the values of W_{HK}, A_{1HK} and H_{HK} values are given. The values of W_{HK} are negative for all samples. Microhardness values, that are calculated according to the Hays–Kendall (HK) model, are outside the plateau region. Therefore, this model is not sufficient for determination of the hardness. Until now, among the applied models for samples showing the RISE behavior, microhardness values can not be reached to the plateau region. Finally, indentation induced cracking (IIC) model, that is developed for samples showing RISE behaviour in the literature, is used to analyse the mechanical properties of undoped and Ru doped samples.

In RISE behavior, hardness of the samples increases with applied loads. Although observing this behavior in various samples, the reason still not fully explained. There are different approaches in the literature. It is expressed that metallic samples can be hardener during the loading and there may occur some cracks in fragile samples during the loading of the indenter. According to Feltham and Banerjee; this behavior is related to energy loss due to some comminutions occurred around the indenter [39]. Because the slit in the sample causes the formation of a smaller size and thus higher microhardness values can be obtained with applying load during the indentation process [40–42].

3.4.3.2 Indentation-induced cracking (IIC) model IIC model is developed to explain the RISE behavior in the samples [43]. According to the model, the applied test load is offset by the total resistance of the sample at maximum depth. This resistance consists from four components: (1) shift of sample or indenter at the interfaces, (2) elastic deformation, (3) plastic deformation and (4) cracks in sample.

According to this model, while the friction and elastic effects led to normal ISE behavior, indentation cracks led to RISE behavior. Li and Bradt reported the importance of the elastic and frictional effects in the PSR model.

Eqn. 14 is directly related with true microhardness for materials showing RISE behavior. Indentation-induced specimen cracking model is the most suitable model for understanding the mechanical properties of materials showing RISE behavior. Determining the precise indentation depth, h, is very important while applying load on the surface of the material. Microhardness can also be calculated with using indentation size and h values depending on d in this model. Namely, indentation depth (h) is directly related with the indentation size after load remove. A part of elastic strain energy in the sample releases with the formation of indentation cracking. Consequently, elastic recovery reduces. Furthermore, cracks usually occurs at high loads where the elastic contribution is not significant [44]. The hardness value in this model can be expressed as [45]

$$H_v = \lambda_1 K_1 \left(\frac{F}{d^2}\right) + K_2 \left(\frac{F^{\frac{5}{3}}}{d^3}\right) \tag{14}$$

here d is the trace's diameter and λ_1, K_1 and K_2 are constants. While, K_2 value is dependent on the applied load, K_1 value is dependent on the geometry of the indenter. While, $H_v = K_1$

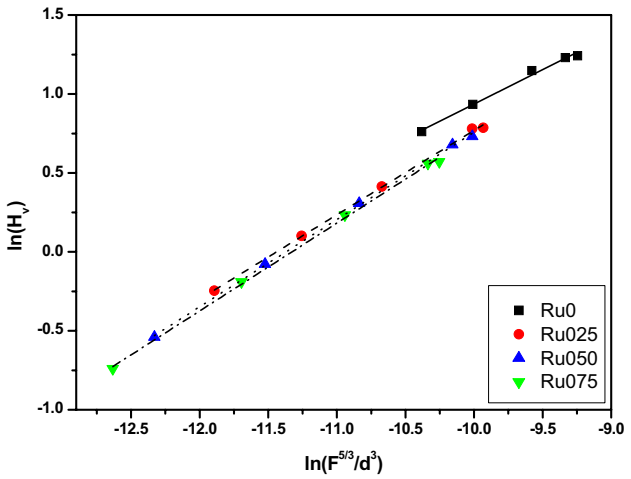

Fig. 9 Variation of $In(H_v)$ with $In(F^{5/3}/d^3)$ according to IIC model for all samples

Table 8 Best-fit results of experimental data according to IIC model

Samples	m	$K \times 10^4$ ($N^{(3-5\,m)/3}/\mu m^{(2-3\,m)}$)	H_{IIC} (GPa)	H_V (GPa)
Ru0	0.436	0.0102	3.458	3.421–3.464
Ru025	0.534	0.0333	2.158	2.182–2.195
Ru050	0.552	0.0414	1.952	1.973–2.080
Ru075	0.556	0.0434	1.886	1.752–1.769

(F/d^2), $\lambda_1 = 1$ and K_2 $(F^{5/3}/d^3) = 0$ for ideal plastic materials, $H_v = K_2$ $(F^{5/3}/d^3)$ and $\lambda_1 = 0$ for ideal brittle solids. If the investigated material is a brittle material only second part of the equation is used,

$$H_v = K\left(\frac{F^{\frac{5}{3}}}{d^3}\right)^m \tag{15}$$

Values of K and m are load independent constants and are obtained from the $In(H_v)$–$In(F^{5/3}/d^3)$ graph (Fig. 9). m is used to determine the ISE or the RISE behaviors. If $m > 0.6$ the material shows a normal ISE behavior, however if $m < 0.6$ the material shows RISE behavior [46]. These values are given in the Table 8. According to the microhardness results, we can conclude that, IIC model gives the most appropriate results for $Bi_{1-x}Ru_xPb_{0.2}Sr_2CaCu_2O_{10+\delta}$ samples (Table 9).

In addition, Fig. 9 shows the results of the application of the IIC model to the data from the four different samples shown in Fig. 3. Despite the significant differences in microhardness values, as well as the varying trends of applied load, it is seen that all of the results fall on a single curve. This confirms that the RISE is directly associated with the indentation-induced specimen cracking. It is confirmed that the RISE occurs because of IIC [44, 47].

4 Conclusion

In this study, the effects of Ru doping on the micromechanical and microstructural properties of $Bi_{1.8-x}Ru_xPb_{0.2}Sr_2CaCu_2O_y$ ($x = 0.0$, 0.025, 0.050, 0.075) system are investigated. Obtained results are listed below.

1. It is shown from XRD analyses that, the main phase is $Bi_{1.6}Pb_{0.4}Sr_2CaCu_2O_x$ (045-0676-ICDD) for the undoped sample. When XRD patterns are investigated, it is shown that there are many phases such as Bi-2212 (045-1058-ICDD), Bi-2201 (047-0737-ICDD) phases seperated from main structure and Sr_3PbO (083-1866-ICDD), $SrBi_4O_7$ (046-0752-ICDD) and $Ca_6Sr_8Cu_{24}O_{41}$ (048-1502-ICDD) impurity phases.
2. All samples have tetragonal structure. Lattice parameters a and c generally decrease with doping.
3. A reduction is observed in the crystallinity of the sample by SEM analyses. As a result, plate and needle-like structure occurs in only undoped sample. The increase in Ru doping does not affect the formation of needle-like structures.
4. The microhardness tests of produced samples are analyzed using Vickers microhardness method. According to the microhardness results, it is found that microhardness depend on applied load. All samples exhibit RISE behavior.

Table 9 The load-dependent Vickers microhardness values at the plateau region and load-independent hardness values calculated using PSR, EPD, HK and IIC models

Samples	H_{PSR} (GPa)	H_{EPD} (GPa)	H_{HK} (GPa)	H_{IIC} (Gpa)	H_V (GPa) (plateau region)
Ru0	4.302	4.434	3.708	3.458	3.421–3.464
Ru025	3.708	4.416	2.725	2.158	2.182–2.195
Ru050	4.024	5.268	2.781	1.952	1.973–2.080
Ru075	3.412	4.434	2.355	1.886	1.752–1.769

5. Values of Vickers microhardness increase with increasing the applied load. Values of *E, Y* and K_{IC} parameter values increase with increasing the hardness. At the same time, values of Vickers microhardness, elastic modulus and yield strength decrease with Ru doping.
6. Experimental results of Vickers micro-hardness are analyzed by using the Meyer's law, the PSR model, the EPD model, the HK approach and the IIC model in literature. All results supports the RISE behavior. The microhardness values increase with increasing the applied load. Finally, IIC model is determined as the most successful model for describing the mechanical properties of our samples.

In this study, effect of Ru substitution ratio on the mechanical and structural properties of BSCCO system, that is prepared in the ratios of x = 0.0, 0.025, 0.050, 0.075, is investigated. Samples are prepared with glass ceramic method. In our future study, we will prepared this samples using solid state reaction and sol–gel methods. And materials, prepared these methods, will be compared in terms of structural, electrical and mechanical properties. Our aim is find the optimum method of material production. Especially, mechanical characterizations are very important for industrial applications.

References

1. L. Arda, O. Ozturk, E. Asikuzun, S. Ataoglu, Structural and mechanical properties of transition metals doped ZnMgO nanoparticles. Powder Technol. **235**, 479–484 (2013)
2. O. Sahin, O. Uzun, U. Kolemen, B. Duzgun, N. Ucar, Indentation size effect and microhardness study of β-Sn single crystals. Chin. Phys. Lett. **22**, 3137 (2005)
3. Y. Yoshino, A. Iwabuchi, R. Onodera, A. Chiba, K. Katagiri, T. Shimizu, Vickers hardness properties of structural materials for superconducting magnet at cryogenic temperatures. Cryogenics. **41**, 505–511 (2001)
4. E.M. Onitsch, Mikroskopie. **2**, 131–151 (1947)
5. H. Li, R.C. Bradt, The microhardness indentation load/size effect in rutile and cassiterite single crystals. J. Mater. Sci. **28**, 917–926 (1993)
6. P.P. Maharjan, Q. Chen, L. Zhang, O. Adebanjo, N. Adhikari, S. Venkatesan, P. Adhikary, B. Vaagensmith, Q. Qiao, Photovoltaic devices and characterization of a dodecyloxybenzothiadiazole-based copolymer. Phys. Chem. Chem. Phys. **18**, 23628–23637 (2016)
7. K.R. Reddy, B.C. Sin, C.H. Yoo, W. Park, K.S. Ryu, J.S. Lee, Y. Lee, A new one-step synthesis method for coating multi-walled carbon nanotubes with cuprous oxide nanoparticles. Scripta Mater. **58**, 1010–1013 (2008)
8. Y.P. Zhang, S.H. Lee, K.R. Reddy, A.I. Gopalan, K.P. Lee, Synthesis and characterization of core-shell SiO_2nanoparticles/poly(3-aminophenylboronic acid) composites. J. Appl. Polym. Sci. **104**, 2743–2750 (2007)
9. K.R. Reddy, K.P. Lee, A.I. Gopalan, Self-assembly directed synthesis of poly(ortho-toluidine)-metal(gold and palladium) composite nanospheres. J. Nanosci. Nanotechnol. **7**, 3117–3125 (2007)
10. A.M. Showkat, Y.P. Zhang, M.S. Kim, A.I. Gopalan, K.R. Reddy, K. Lee, Analysis of heavy metal toxic ions by adsorption onto amino-functionalized ordered mesoporous silica. Bull. Korean Chem. Soc. **28**, 1985–1992 (2007)
11. K.R. Reddy, K. Nakata, T. Ochiai, T. Murakami, D.A.. Tryk, A. Fujishima, Facile fabrication and photocatalytic application of Ag nanoparticles-TiO_2 nanofiber composites. J. Nanosci. Nanotechnol. **11**, 3692–3695 (2011)
12. M. Hassan, E. Haque, K.R. Reddy, A.I. Minett, J. Chen, V.G. Gomes, Edge-enriched graphene quantum dots for enhanced photo-luminescence and supercapacitance. Nanoscale **6**, 11988–11994 (2014)
13. K.R. Reddy, V.G. Gomes, M. Hassan, Carbon functionalized TiO_2 nanofibers for high efficiency photocatalysis. Mater. Res. Express **1**, 015012 (2014)
14. M. Cakici, R.R. Kakarla, F. Alonso-Marroquin, Advanced electrochemical energy storage supercapacitors based on the flexible carbon fiber fabric-coated with uniform coral-like MnO_2 structured electrodes. Chem. Eng. J. **309**, 151–158 (2017)
15. K.R. Reddy, K.P. Lee, A.I. Gopalan, Self-assembly approach for the synthesis of electro-magnetic functionalized Fe_3O_4/polyaniline nanocomposites: effect of dopant on the properties. Colloid Surf. A **320**, 49–56 (2008)
16. O. Ozturk, T. Gokcen, S. Cavdar, H. Koralay, A. Tasci, A study on nucleation, crystallization kinetics, microstructure and mechanical properties of Ru–Bi partial substituted BSCCO glass ceramics. J. Therm. Anal. Calorim. **123**, 1073–1082 (2016)
17. H. Koralay, O. Hicyilmaz, S. Cavdar, E. Asikuzun, A. Tasci, O. Ozturk, Effect of Zn content on microstructure and mechanical performance in $Bi_{1.8}Sr_2Ca2Cu_{3.2-x}Zn_xO_{10+\delta}$ glass ceramic. J. Mater. Sci.: Mater. Electron. **25**, 3116–3126 (2014)
18. O. Ozturk, E. Asikuzun, S. Kaya, G. Yildirim, M. Turkoz, A. Kilic, Improvement of the nature of indentation size effect of Bi-2212 superconducting matrix by doped Nd inclusion and theoretical modeling of new matrix. J. Supercond. Novel Magn. **27**, 1403–1412 (2014)
19. E. Asikuzun, O. Ozturk, H.A. Cetinkara, G. Yildirim, A. Varilci, M. Yilmazlar, C. Terzioglu, Vickers hardness measurements and some physical properties of Pr_2O_3 doped Bi-2212 superconductors. J. Mater. Sci.: Mater. Electron. **23**(5), 1001–1010 (2012)
20. W.C. Oliver, G.M. Pharr, An improved technique for determining hardness and elastic modulus using load and displacement sensing indentation experiments. J. Mater. Res. **7**, 1564–1583 (1992)
21. D. Tabor, The hardness and strength of metals. J. Inst. Met. **79**, 1–18 (1951)
22. M. Yilmazlar, H.A. Cetinkara, M. Nursoy, O. Ozturk, C. Terzioğlu, Thermal expansion and Vickers hardness of $Bi_{1.6}Pb_{0.4}Sr_2Ca_{2-x}Sm_xCu_3O_y$ superconductors. Physica C **442**, 101 (2006)
23. U. Kölemen, O. Uzun, M.A. Aksan, N. Güçlü, E. Yakıncı, An analysis of load depth-sensing microindentation experiments for intermetallic MgB_2. J. Alloy. Compd. **415**, 294–299 (2006)
24. H. Aydın, C. Terzioglu, Mechanical and superconducting properties of $Bi_{1.8}Pb_{0.35}Sr_{1.9}Ca_{2.1}Cu_3\ Gd_xO_y$. Chin. J. Phys. **47**, 192–206 (2009)
25. X. Chu, S.A. Barnett, Model of superlattice yield stress and hardness enhancements. J. Appl. Phys. **77**, 4403 (1995)
26. O. Ozturk, G. Yildirim, E. Asikuzun, M. Coskunyurek, M. Yilmazlar, A. Kilic, Change of formation velocity of Bi-2212 superconducting phase with annealing ambient. J. Mater. Sci.: Mater. Electron. **24**, 4643–4654 (2013)
27. J. Gong, J. Wu, Z. Guan, Examination of the indentation size effect in low-load Vickers hardness testing of ceramics. J. Eur. Ceram. Soc. **19**, 2625–2631 (1999)

28. A. Elmustafa, D. Stone, Nanoindentation and the indentation size effect: Kinetics of deformation and strain gradient plasticity. J. Mech. Phys. Solids **51**, 357–381 (2003)
29. K. Sangwal, On the reverse indentation size effect and microhardness measurement of solids. Mater. Chem. Phys. **63**, 145–152 (2000)
30. Y. Matsuo, H. Sasaki, Effect of grain size on microcracking in lead titanate ceramics., J. Am. Ceram. Soc. **49**, 229–230 (1966)
31. O. Ozturk, E. Asikuzun, S. Kaya, Significant change in micro mechanical, structural and electrical properties of MgB2 superconducting ceramics depending on argon ambient pressure and annealing duration. J. Mater. Sci.: Mater. Electron. **26**, 3840–3852 (2015)
32. A. Leenders, M. Mich, H. Freyhard, Influence of thermal cycling on the mechanical properties of VGF melt-textured YBCO. Physica C **279**, 173–180 (1997)
33. M. Yilmazlar, O. Ozturk, O. Gorur, I. Belenli, C. Terzioglu, Role of diffusion-annealing time on the mechanical properties of bulk Bi-2223 superconductors diffusion-doped with Au. Supercond. Sci. Technol. **20**, 365 (2007)
34. M. Yilmazlar, H. Cetinkara, M. Nursoy, O. Ozturk, C. Terzioglu, Thermal expansion and Vickers hardness measurements on $Bi_{1.6}Pb_{0.4}Sr_2Ca_{2-x}Sm_x$ Cu_3O_y superconductors. Physica C **442**, 101–107 (2006)
35. H. Aydın, A. Babanli, S.P. Altintas, E. Asikuzun, N. Soylu, O. Ozturk, M. Dogruer, C. Terzioglu, G. Yildirim, Breaking point of the harmony between Gd diffused Bi-2223 slabs with diffusion annealing temperature. J. Mater. Sci.: Mater. Electron. **24**, 4566–4573 (2013)
36. S. Celik, O. Ozturk, E. Coşkun, M. Sarıhan, E. Asikuzun, K. Ozturk, C. Terzioglu, Analysis of indentation size effect (ISE) behavior in low-load Vickers microhardness testing of $(Sm123)_{1-x}(Nd123)_x$ superconductor system. J. Mater. Sci.: Mater. Electron. **24**, 2218–2227 (2013)
37. G.P. Upit, S.A. Varchenya, Microhardness of alkali halide crystals. Phys. Status Solidi B **17**, 831–835 (1966)
38. S.J. Bull, T.F. Page, E.H. Yoffe, An explanation of the indentation size effect in ceramics. Philos. Mag. Lett. **59**, 281–288 (1989)
39. C. Hays, E. Kendall, An analysis of Knoop microhardness. Metallography **6**, 275–282 (1973)
40. P. Feltham, R. Banerjee, Theory and application of microindentation in studies of glide and cracking in single crystals of elemental and compound semiconductors. J. Mater. Sci. **27**, 1626–1632 (1992)
41. E. Asikuzun, A. Donmez, L. Arda, D. Akcan, O. Ozturk, O. Cakiroglu, M. Tosun, S. Ataoglu, C. Terzioglu, Structural and mechanical properties of (Co/Mg) Co-doped nano ZnO. Ceram. Int. **41**, 6326–6334 (2015)
42. M. Tosun, S. Ataoglu, L. Arda, O. Ozturk, E. Asikuzun, D. Akcan, O. Cakiroglu, Structural and mechanical properties of ZnMgO nanoparticles. Mater. Sci. Eng. A **590**, 416–422 (2014)
43. M.B. Turkoz, S. Nezir, O. Ozturk, E. Asikuzun, G. Yildirim, C. Terzioglu, A. Varilci, Experimental and theoretical approaches on mechanical evaluation of Y123 system by Lu addition. J. Mater. Sci.: Mater. Electron. **24**, 2414–2421 (2013)
44. H. Li, R.C. Bradt, The effect of indentation-induced cracking on the apparent microhardness. J. Mater. Sci. **31**, 1065–1070 (1996)
45. B.R. Lawn, M.V. Swain, Microfracture beneath point indentations in brittle solids. J. Mater. Sci. **10**, 113–122 (1975)
46. B.R. Lawn, E.R. Fuller, Equilibrium penny-like cracks in indentation fracture. J. Mater. Sci. **10**, 2016–2024 (1975)
47. R. Awad, A.A. Aly, M. Kamal, M. Anas, Mechanical properties of $(Cu_{0.5}Tl_{0.5})$-1223 substituted by Pr. J. Supercond. Novel Magn. **24**, 1947–1956 (2011)